 doi:10.20944/preprints202209.0448.v1

Article

Nanoscale Printing of Indium-Tin-Oxide by Femtosecond Laser Pulses

Jingwen Hu,[1, a)] Zhen-Ze Li,[2] Yang-Yang Zhao,[2] Yi-Shi Xu,[2] Lin Wang,[2] Molong Han,[1, 3] Lachlan Hyde,[4] Soon Hock Ng,[1, 3, b)] Lei Wang,[2, c)] and Saulius Juodkazis[1, 5]

[1)] *Optical Sciences Centre and ARC Training Centre in Surface Engineering for Advanced Materials (SEAM), School of Science, Swinburne University of Technology, Hawthorn, Vic 3122, Australia*

[2)] *State Key Laboratory of Integrated Optoelectronics, College of Electronic Science and Engineering, Jilin University, Changchun, 130012, China*

[3)] *Melbourne Centre for Nanofabrication (MCN-ANFF), 151 Wellington Rd, Clayton Vic 3168, Australia*

[4)] *Space Technology and Industry Institute, Graphene Certification Labs, Swinburne University of Technology, Hawthorn, Vic 3122, Australia*

[5)] *World Research Hub Initiative (WRHI), School of Materials and Chemical Technology, Tokyo Institute of Technology, 2-12-1, Ookayama, Meguro-ku, Tokyo 152-8550, Japan*

(Dated: 23 September 2022)

Deposition/printing of materials with sub-1 μm precision and size (cross sections) is required for optical and electrical micro-devices. Crystalline c-ITO (Indium tin oxide) nanostructures were patterned on glass with a precision that formed gaps of 20-50 nm between individual disks or lines of $\sim$ 250 nm diameter or width. The absorbed energy density [J/cm^3] followed the second order dependence on pulse energy. This facilitated high resolution and precision for nanoscale laser writing at the 515 nm laser wavelength. Patterns for optical elements such as circular gratings and micro-disks were laser printed using ITO as a resist. Unexposed amorphous a-ITO was chemically removed in aqueous 1% vol. HF solution. This use of a-ITO as solid-resist is promising for metamaterial and micro-optical applications.

Keywords: IR; laser printing; ITO; solid resist

I. INTRODUCTION

Indium tin oxide (ITO) is an n-type semiconductor with a 3.5-3.7 eV bandgap that is transparent under visible light from 390 nm to 700 nm wavelengths (3.2-to-1.8 eV), has refractive a index of $n \approx 1.5$, and an extinction coefficient of $\kappa < 0.005$ [1]. Its electrical conductivity is attributed to the Sn dopant; ITO is diamagnetic[2]. ITO is currently widely used in transparent display devices, transparent coatings for photovoltaics such as solar cells, organic light-emitting devices (OLEDs), photo diodes, and photo transistors due to its high transmittance and relatively high conductivity[3,4]; the electron density is $n_e \sim 10^{19}$ cm^{-3}. In the near-IR spectral window of $\lambda = 1.1 - 1.3$ μm, ITO is an epsilon-near-zero (ENZ) $\varepsilon \equiv (n + i\kappa)^2 \to 0$ material[5]. The ENZ condition opens up possibilities of tailoring energy deposition in perfect absorbers and exploiting it for metamaterial applications and nonlinear optics[6–9]. The highest transmission of 2D ITO $T > 99\%$ and sheet resistance of 5.4 k$\Omega/\square$[10] was demonstrated using low temperature liquid metal synthesis[11]. This opens up wider opportunities for flexible electronics and optics, including wearables and sensors.

[a)] Electronic mail: J.H. and Z.L. contributed equally.
[b)] Electronic mail: (Corresponding author) soonhockng@swin.edu.au
[c)] Electronic mail: (Corresponding author) leiwang1987@jlu.edu.cn

Preprints (www.preprints.org) | NOT PEER-REVIEWED | Posted: 29 September 2022 doi:10.20944/preprints202209.0448.v1

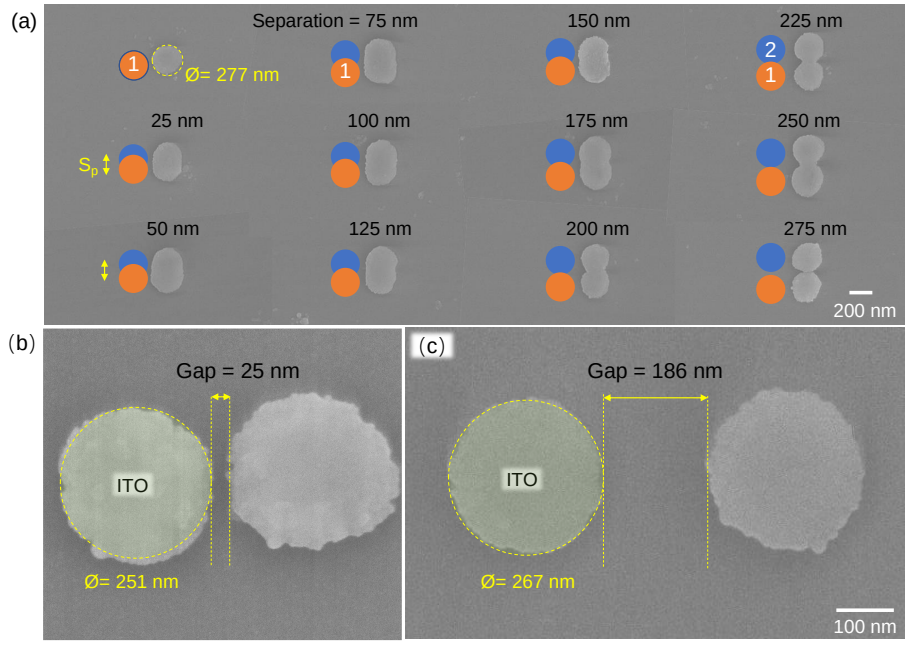

FIG. 1. SEM images of ITO structures by nano-printing. (a) Two pulse-burst exposure of ITO film after wet-etch in 1% vol. HF solution for 5 seconds. The ITO was printed by two laser pulse-bursts (515 nm/280 fs/10 pulses per burst/ pulse energy $E_p = 0.92 \pm 0.02$ nJ (on sample)) at different separation S_p from 0 to 300 nm. Focusing was with $NA = 0.9$ objective lens; polarisation linear (horizontal). Nanogaps can be controlled from 25-nm (b) to ten times larger (c). Numerical aperture of the objective lens was $NA = 0.9$ (focal spot diameter $\oslash = 1.22\lambda/NA = 698$ nm), thickness of ITO films $d \approx 60$ nm. Polarisation of laser pulses (b,c) was linear (vertical).

It is established that the electrical properties of ITO films rely on the film deposition and annealing conditions. The amorphous (a-ITO) and crystalline (c-ITO) phases of ITO have different resistivities, owing to lattice arrangement varying the carrier density[12]. It was shown that ITO can be used as a negative tone resist by writing patterns in glass using a sub-15 fs laser and subsequently etching in a 10% hydrochloric acid solution[13]. Sub-1 μm-wide ITO lines down to 50 nm were demonstrated by scanning a focused fs-laser beam[13–15]. Sub 100 nm ripple structures were also fabricated by controlling the polarisation in concert with the writing direction[16]. Previous studies have shown that laser irradiation of a-ITO induces crystallisation [14,17,18]. These c-ITO regions exhibit a different selectivity to the a-ITO, etching more slowly in both HCl and Fe_3-HCl etchants[17,19,20]. Recently, the use of nano-films as a solid resist in combination with laser direct writing for negative and positive tones has gained interest[21,22].

In this study, amorphous a-ITO films were modified by sub-1 ps laser pulses with deep-sub-wavelength precision and resolution. Nanoscale modification via localised annealing and structural modification/crystallisation leading to c-ITO was demonstrated. By meticulously controlling the fs-laser fluence below the ablation threshold, modified ITO on a sub-wavelength scale was created, which could withstand wet etching in an aqueous HF solution. This provides the possibility of directly writing not just lines, but sub-wavelength patterns and individual nano-particles with controlled size and spacing. Nano-disks and arrays with diameter ~250 nm and nanogaps as small as 25 nm were fabricated with high resolution and controllability, with the focus towards metamaterials and micro-optics.

 doi:10.20944/preprints202209.0448.v1

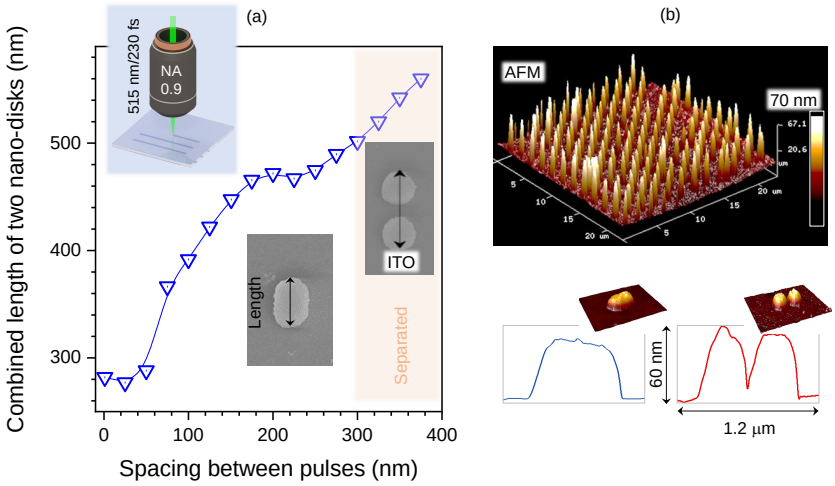

FIG. 2. (a) Plot showing the length of two pulse-burst exposed ITO nano-disks vs. separation between two these bursts S_p measured by SEM images. (b) AFM profilometry of laser printed nano-disks. Two pulse-burst exposure of ITO film after wet-etch in HF solution. Polarisation of laser E-field was horizontal, $NA = 0.9$, pulse energy $E_p = 0.92 \pm 0.02$ nJ (on sample), $N = 10$ pulses burst per disk at $f = 5$ kHz (for the two-spots exposure).

II. RESULTS AND DISCUSSION

Direct laser writing/printing of nano-disks/lines were carried out at the second harmonic wavelength of $\lambda = 515$ nm (photon energy $h\nu = 2.407$ eV), which didn't have a ns-long pedestal pulse background due to emission of an excitation diode pulse radiation. This is important since very small pulse energies $E_p \sim 0.7$ nJ were used and long background emission at the fundamental wavelength would cause significant absorption in ITO (In_2O_3-SnO_2). At the laser excitation wavelength, ITO has index $\tilde{n} \equiv 1.8983 + i3.6549 \times 10^{-3}$ or permittivity $\varepsilon \equiv \tilde{n}^2 = 3.6036 + i0.013876$ corresponding to the absorption coefficient $\alpha = 4\pi\kappa/\lambda = 891.83$ cm^{-1}.[23] Even with such strong absorption, an estimate of transmittance $T = 10^{-\alpha d} \approx 98.8\%$ for a $d = 60$ nm thickness ITO film (reflectance is not taken into account, $R = 0$ for this qualitative estimate). This shows that linear absorbance was negligible and nonlinear light-matter interaction was important for the following laser writing/printing.

A. Single nano-disks and pairs

Figure 1(a) shows scanning electron microscopy (SEM) images of patterned ITO disks made by two laser pulse-bursts of $N = 10$ pulses (230 fs/515 nm) at the laser pulse energy of $E_p = 0.92$ nJ and laser repetition rate of $f = 1$ kHz with subsequent chemical etching. Focus was placed onto the 60-nm-thick amorphous a-ITO surface and HF etching was used to remove un-exposed ITO. Two bursts positions with separation S_p from 0 to 300 nm was used. The irradiated region was recognisable in SEM imaging due to different charging characteristics, however, the disk structure was only revealed after development in aqueous 1% vol. HF solution. Laser irradiation changed a-ITO and rendered it less soluble in the HF solution. It was shown previously[12] that the laser energy deposited heated the film, annealing a-ITO into polycrystalline c-ITO. This caused different etching rates between amorphous and crystalline ITO (Fig. 1). A small pulse energy, $E_p \approx 0.7$ nJ (and $N = 10$ pulse dose), is required to turn a-ITO into HF insoluble c-ITO. This energy, focused onto a $\oslash \equiv 2r = 1.22\lambda/NA \approx 700$ nm spot, corresponds to a fluence of $F_p = E_p/(\pi r^2) \approx$

Preprints (www.preprints.org) | NOT PEER-REVIEWED | Posted: 29 September 2022 doi:10.20944/preprints202209.0448.v1

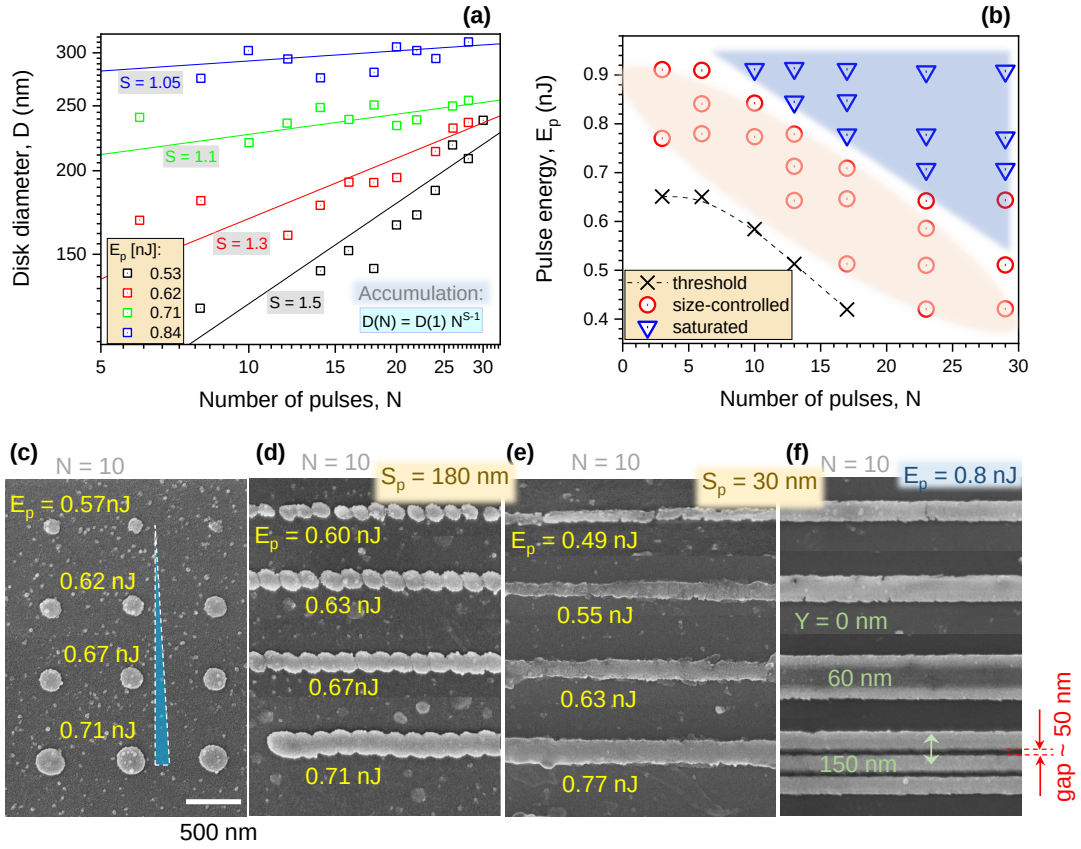

FIG. 3. (a) Plot showing the diameter of nano-disk as a function of pulse number N measured by SEM for the pulse energy between $E_p = 0.77$ nJ and 0.46 nJ. (b) A E_p vs N diagram for nano-disk fabrication: threshold of disk formation ($\times$), region where different sized disks can be made ($\circ$) and where size (diameter) saturates ($\triangledown$). (c-d) c-ITO single dots separated and connected into a line on glass recorded at different pulse energies E_p for $N = 10$ per irradiation site. (e) Formation of lines of different widths by selection of E_p, N, and separation S_p along the line. (f) Pattern of separate lines using vertical Y shift. Polarisation linear (horizontal; along the line).

0.18 J/cm^2 per pulse and an irradiance (average) of $I_p = F_p/t_p \approx 0.79$ TW/cm^2 (where pulse duration was $t_p = 230$ fs and numerical aperture of the objective lens was $NA = 0.9$). Double the fluence ($E_p \approx 1.4$ nJ) was enough to ablate sub-diffraction holes of 200 nm in the 60-nm-thick ITO film (not shown here).

The blue and orange circles in Fig. 1(a) depict how two irradiation sites were arranged with different separation. The top-left nano-disk of 277 nm diameter was irradiated by a single burst of $N = 10$ pulses. With an increasing of spacing S_p, the outside contour of nano-disk pattern stretches to an ellipse then to a gourd shape eventually two nano-disks become separated completely. A narrow gap of 25 nm width was opened between two nano-disks (Fig. 1(b)). The distance between two nano-disks of 250 ± 20 nm diameter can be well controlled and structure length can be defined (Fig. 2(a)). There was no clear elongation of nano-disks along orientation of polarisation. This can be attributed to the low anisotropy of heat transfer (by electrons) during the pulse, which can be considerable in homogeneous and crystalline materials[24] or due to the vectorial nature of focusing at high NA[25]. The surface morphology of a dots matrix pattern can be defined (Fig. 1(b)). The height of ITO disks were approximately 60 nm, which is the thickness of the a-ITO film. The separation of nano-disks were evident from AFM cross sections (Fig. 2(b)).

 doi:10.20944/preprints202209.0448.v1

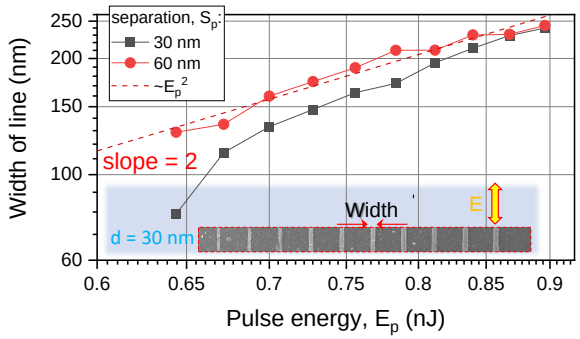

FIG. 4. Plot showing the evolution of line width vs pulse energy E_p for $N = 10$ pulses per site at different separations S_p along the line (a log-log plot); polarisation of E-field was linear (along the line) shown in the inset. The trend of dependence is closely following a nonlinear $\propto E_p^2$ dependence.

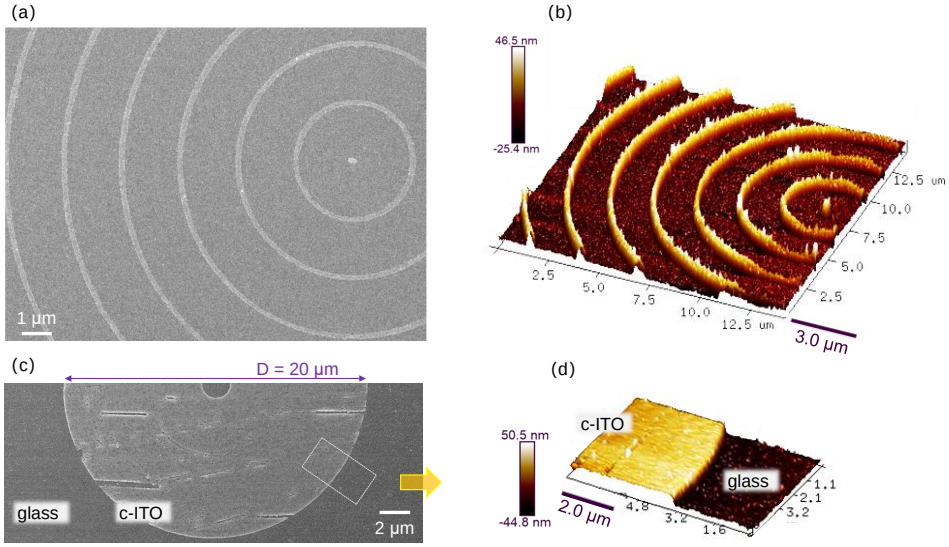

FIG. 5. (a) SEM image of a bessel-beam generating micro-optical element recorded on glass. Polarisation of laser E-field was horizontal, $NA = 0.9$, scanning speed $v_s = 30$ μm/s and pulse energy $E_p = 0.9$ nJ (on sample. (b) AFM view of the concentric grating with ITO lines of 60 nm height. (c) Bulk c-ITO on glass recorded on glass. d) AFM view of the bulk of ITO.

B. From lines with nano-gaps to optical micro-elements

Figure 3(a) summarises the effect of laser pulse energy E_p and dose (via pulse number N) for c-ITO pattern formation. By incrementing the number of pulses N, the diameter of the disk becomes larger for $E_p = 0.55$ nJ until 0.62 nJ. When the pulse energy reached 0.71 nJ to 0.84 nJ, the diameter saturated at the maximum size of approximately 240 nm to 300 nm after the fifth pulse and became constant for larger N. The pulse energy and pulse number (dose) determine the final diameter D (or $\oslash$) of the nano-disks.

An accumulation effect was present during nano-disk formation. This is where energy deposited from each successive pulse accumulates, in this case, manifesting as a larger diameter as the number of pulses N increases. As usual for accumulation effects, one can apply the dependence $\oslash(N) = \oslash(1) \times N^{S-1}$, where $\oslash(1)$ is the initial diameter of disk after

Preprints (www.preprints.org) | NOT PEER-REVIEWED | Posted: 29 September 2022 doi:10.20944/preprints202209.0448.v1

$N = 1$ pulses and $0 < S \leq 1$ is the accumulation exponent; when $S = 1$ the effect of a multi-pulse exposure has no cumulative effect. The accumulation exponent changed from $S = 1.5$ to 1.05 from the lowest to the largest pulse energies (0.5 - 0.9 nJ) as shown in Fig. 3(a). The maximum disk diameter was $\oslash$ =300 nm, after which it became independent on E_p and N. A further increase to $E_p \geq 0.91$ nJ caused ablation of a nano-hole. Three different conditions for nano-disk formation can be distinguished as shown in Fig. 3(b). At the threshold of the E_p vs. N plot, nano-disks form with the minimum diameter $\oslash$. The working region, when the diameter can be controlled by the exposure dose $\oslash(E_p, N)$, is the most useful (circle markers $\circ$). When $E_p = 0.46$ nJ, a nano-disk of $\oslash = 100$ nm diameter appears after $N > 15$ pulses and the accumulation effect is strongest ($S > 1.5$).

Figures 3(c-f) demonstrate flexibility of position and size control over the disk pattern as well as formation of fine lines of different widths and separation. No c-ITO formed when the pulse energy was lower than 0.46 nJ even for a $N > 100$ dose (at $f = 10$ kHz repetition rate). The minimum diameter of c-ITO nano-disk was approximately 100 nm and the maximum 300 nm. Ablation ripples appeared at the centre of focus for a large dose which was an unwanted result for this dot/line printing. When distance the between adjacent focal spots changed from 30-to-150 nm (along the line), a line pattern developed with wavy-to-smooth edges which was exposure dose dependent. At each exposure site (disk), the laser repetition rate was $f = 5$ kHz and the number of pulses in a burst was $N = 10$. The shutter was closed during travel between each site. Due to the long break between two bursts (scan velocity of $v_s = 1.15$ μm/s), the ITO modification at a preceding site finished before the next, resulting in a wavy edged line, dependent on the separation between exposure sites.

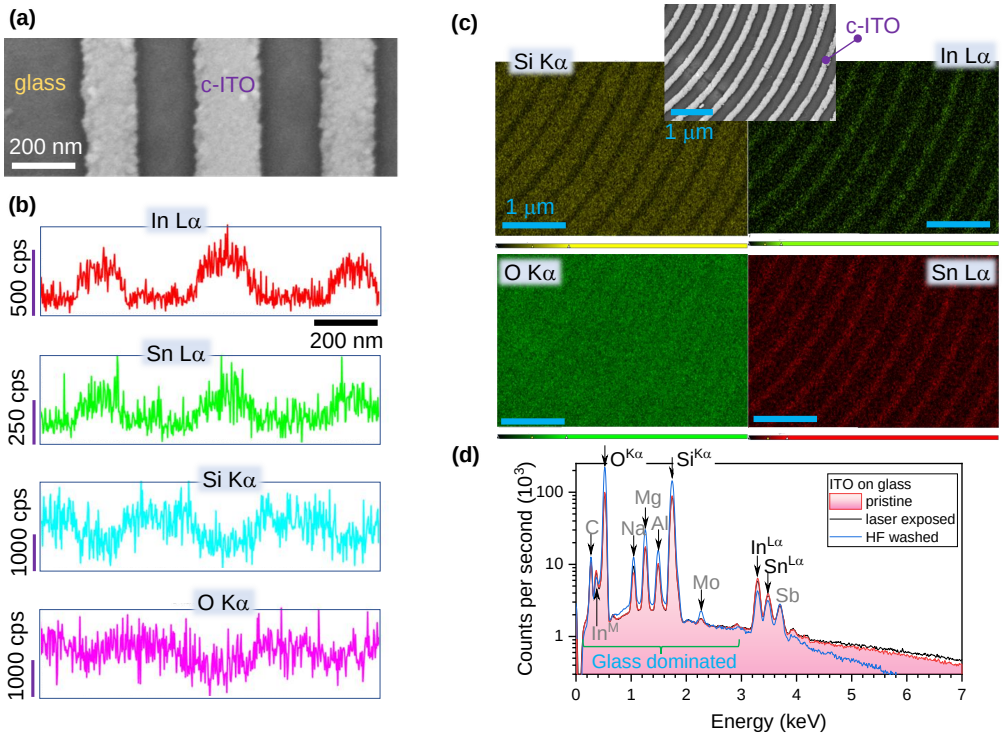

FIG. 6. X-ray energy dispersion spectroscopy (EDS) analysis of c-ITO structure. (a) SEM image of c-ITO line structure after laser exposure and development. (b) Distribution of Si ($K_\alpha = 1.739$ keV), O ($K_\alpha = 0.525$ keV), In, Sn according their characteristic lines; 200 nm scale bar is same for all elemental maps. (c) Compositional maps of the four elements on the surface of sample. Inset shows SEM image of the mapped surface; all same 1 μm scale bar. (d) The EDS spectra of pristine, laser irradiated and HF-developed ITO structures.

Preprints (www.preprints.org) | NOT PEER-REVIEWED | Posted: 29 September 2022 doi:10.20944/preprints202209.0448.v1

Polarisation was linear orientated parallel to the scanning path. The narrowest lines were ~ 90 nm close to the smallest diameter of the disks at ~ 100 nm. Gaps of ~ 50 nm between lines were made by the described $N = 10$ pulse exposure per irradiation site (Fig. 3(f)).

Interestingly, the diameter of the disk depended on the pulse energy E_p in a nonlinear way, as apparent from Fig. 3(c). For a line, patterned using the same $N = 10$ pulses per site and with $S_p = 30, 60$ nm, the width closely followed a 2^{nd} power law dependence $Width \propto E_p^2$ as shown in Fig. 4. Since pulse energy E_p, fluence F_p, dose D_p, and intensity (irradiance) I_p are all proportional to each other, such scaling would imply that nano-disks and lines were formed by two photon absorption (TPA). Indeed, $2h\nu = 4.814$ eV which is larger that the ITO bandgap of ~ 3.7 eV. However, since the initial a-ITO is highly transparent to the 515 nm wavelength used, it was necessary to accumulate several pulses over the same site on 60-nm-thick ITO to render it absorbing. This hints at the importance of absorbed energy density W_{ab} in the volume, i.e., J/cm^3 rather than fluence (or dose) J/cm^2. When the modification is proportional to the instantaneous electron density, n_e, the deposited laser energy density in the volume scales as $W_{ab} \propto \frac{n_e}{n_{cr}} F_p \propto F_p^2$, where n_{cr} is the critical electron density at the wavelength of irradiation[26]. This scaling of energy deposition into volume follows a second order dependence $W_{ab} \propto E_p^2$, since electron density is proportional to the energy (fluence, intensity) $n_e \propto E_p$. The strongest energy deposition into the target/sample takes place where a strongly excited region of material (plasma) exists with the electron density approaching the critical; the intensity used in experiment was high ~ 1 TW/cm^2 and strong ionisation of material takes place. These are ENZ conditions where material turns into $1 > \varepsilon > 0$ ($\varepsilon = 0$ is the dielectric breakdown by definition). These conditions of material excitation are also defined as a dielectric-metal (Die-Met) state of matter[8,27].

Figure 5 shows an example of the fabrication of micro-optical elements: a Bessel-beam generating concentric grating and a micro-disk optical retarder recorded in c-ITO on glass. The width of a single line scan was about 200 nm. A 60 nm height for $n \approx 1.5$ corresponds to 23% wave retardance at 400 nm wavelength (close to $\lambda/4$). Since the width of the c-ITO line was independent of the linear polarisation orientation, symmetric patterns of the same line-width were formed. An area of a c-ITO disk with 20 μm diameter was made with small 100 nm radial steps between concentric line scans (Fig. 5(c-d)). Since a large area was exposed during disk fabrication, it was more susceptible to ablation and ripple formation when compared to parallel lines.

C. Material analysis

Figure 6 summarises the characterisation of the C-ITO pattern by the energy-dispersive X-ray spectroscopy (EDS). Lines of c-ITO with ~ 200 nm gaps obtained after laser printing and HF etching are shown in the SEM image (a). The EDS spectrum (b) shows the corresponding spatial distribution of In, Sn, Si and O measured as cross-section perpendicular to the c-ITO lines. The peaks coincide perfectly with the topography of the ITO lines. In and Sn contributes strongly at the ridge and barely exists between lines (where glass substrate is exposed). On the contrary, Si had a significant contribution between c-ITO lines but was nearly negligible on the c-ITO pattern. Oxygen showed a slight increase on the c-ITO lines due to higher concentration in ITO and a cumulative contribution from the larger depths from the SiO_2-rich glass substrate. Considering that the concentration of Si and O is an order of magnitude larger than that of In and Sn, a spectral window of EDS spectrum was selected for specific elements. Three peaks were expected for the major elements In ($L_\alpha = 3.286$ keV), Sn ($L_\alpha = 3.443$ keV) and Sb ($L_\alpha = 3.604$ keV) which were measured before and after laser exposure as well as after HF etch. Without HF etching, no significant difference was found between pristine and laser exposed samples. Interestingly, the Sn/In ratio of the modified c-ITO pattern area (after HF development) increases by 50% as compared to the non-treated sample. The increase in Sn/In ratio and hence loss of In was observed with Fe_3–HCl etchant and magnetron sputtered then annealed ITO. It was attributed to preferential etching of In_2O_3 due to the negative Gibbs free energy

of the In^{3+} dissociation[20]. The lower bond strength of In−O (≈ 3.73 eV) compared to Sn−O (≈ 5.68 eV) may be broken by multiphoton absorption[28]. These effects likely affect the etch rates during HF exposure, however a dedicated study is outside the scope of this discussion. The low energy side of EDS (Fig. 6(d)) shows larger intensity of peaks after a-ITO is removed, which is an expected result since more glass substrate was exposed and cleaned due to the HF etch.

D. Numerical modeling of light field enhancement

Qualitative insights in the light absorption, scattering, and enhancement at the nanoscale was numerically modeled using the finite difference time domain (FDTD) method (Lumerical, Ansys). The permittivity of ITO was calculated from experimentally measured complex refractive index $\tilde{n}$[23] (Fig. 7(a)). Cross sections of light absorption σ_{ab}, scattering σ_{sc}, and extinction (total loss) $\sigma_{ex} \equiv \sigma_{ab} + \sigma_{sc}$ was calculated using a total field scattered field (TFSF) light source (Fig. 7(b)) for typical nano-disk pairs of 250 nm and 230 nm diameters with 40 nm gap. The light field intensity in the nanogap and at the rim of ITO-disk at the top plane and the ITO-glass interface showed strong field enhancements $E > 10$ (see insets in Fig. 7(b)). Since ITO is transparent at the visible spectral range, a considerable light field enhancement can be created in the interface regions air-ITO and ITO-glass. This is also facilitated by the high refractive index of ITO $n > 1.5$ at shorter wavelengths. The almost linear dispersion of ITO at visible wavelengths (Fig. 7(a)) can be tapped for wavelength-specific light localisation on nanoparticles and metasurfaces. Figure A1 shows the light field enhancement for periodic patterns of nano-disk pairs on a square lattice with a $\Lambda = 1$ μm period under linearly polarised illumination with $|E| = 1$. Apart from expected enhancement inside the gap, also the case for plasmonic nanoparticles, a strong light field localisation on the top-surface as well as at the interface between ITO and glass was observed due to transparency of ITO. This trait, along with its high electrical conductivity can be harnessed with a combination of optical and electrical modalities for characterisation of photo-electrochemical processes, as was shown for surface enhanced Raman scattering

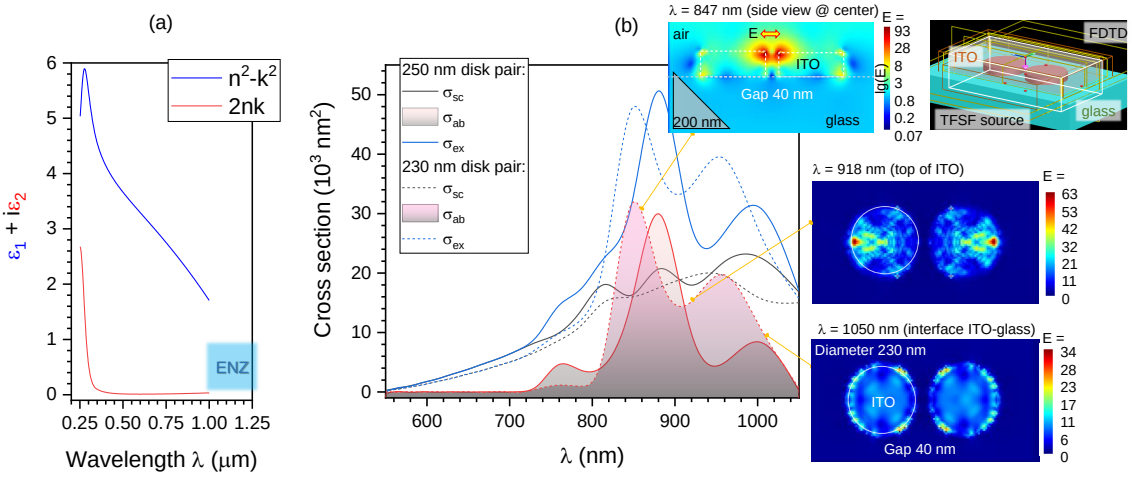

FIG. 7. Numerical modeling of light intensity on an ITO metasurface consisting of nano-disk pairs. (a) Permittivity $\tilde{\varepsilon} \equiv \varepsilon_1 + i\varepsilon_2 \equiv (n + ik)^2$ of ITO[23]. The epsilon-near-zero (ENZ) region $0 < \varepsilon_1 < 1$ is the near-IR spectral region. (b) Cross sections of scattering, absorption and extinction $\sigma_{ex} \equiv \sigma_{ab} + \sigma_{sc}$ for a pair of ITO nanodisks calculated for 250 nm and 230 nm diameters using a total-field scattered-field (TFSF) source in Lumerical. Refractive index of glass $n = 1.4$, the height of disk $h = 80$ nm, gap 40 nm. Insets show characteristic light enhancement maps at different cross-sections and wavelengths. Linear polarisation of light was aligned perpendicular to the gap.

(SERS) using interdigitated micro-electrodes with nanogaps[29]; see Appendix and Fig. A1 for E-field enhancement maps at different wavelengths.

III. CONCLUSIONS AND OUTLOOK

The use of a-ITO as solid resist (negative type) was demonstrated using fs-laser pulses (230 fs/515 nm) tightly focused with a $NA = 0.9$ objective lens into a $\oslash \approx 700$ nm focal spot. Sub-diffraction limited disks with diameters $200 - 300$ nm can be formed by multi-pulse exposure. The accumulation effect, which showed changes in disk diameter based on the number of pulses per burst, was revealed, with a larger exponent $S = 1.5$ at lower pulse energies $E_p \approx 0.5$ nJ. Such nano-disks can be used to define patterns of nanoparticles as well as to write micro-lines with widths considerably smaller than the diffraction limit. EDS confirmed the change of a-ITO into a poly-crystalline form, including a partial loss of In after laser exposure and development in 1% HF solution.

Combining the intricate control over the re-crystallisation a-ITO into c-ITO with glass surface remelting and formation of nano-domes[30], deposition and nano-writing of c-ITO over 3D complex surfaces such as black-Si[31], and atomic layer deposition (ALD) should open applications into 3D nanoscale ITO metasurfaces and will be the focus of future research endeavours. Low fluence exposure and highly localised oxidation of Si using ultra-short laser pulses was shown to act as a negative-tone resist for subsequent plasma etching[32]. The new possibility of using pre-surface modification of thin films and bulk materials as negative (or positive) resists for wet or dry etching is not well explored. It is a promising area of maskless direct-write nanotechnology that is also explored in this study.

IV. EXPERIMENTAL: SAMPLES AND PROCEDURES

The substrates used in the experiments were n-type amorphous a-ITO film deposited by radio-frequency (RF) sputtering and had a ∼60 nm thickness.

Fabrication was carried out with a femtosecond (fs)-laser (Pharos, Light conversion) with $t_p = 230$ fs pulse duration and $\lambda = 515$ nm wavelength at a $f = 5$ kHz repetition rate. The laser beam was focused by an objective lens with a numerical aperture $NA = 0.9$ (Olympus). Pulse energy was measured by a power meter (Thorlabs) with accuracy of 0.01 μW at 10 kHz repetition rate and the energy per pulse E_p (on the sample) was calculated from the power/energy measured in front of the objective lens; in a separate experiment the transmission of the focusing optics was carried out. Fabrication was controlled by high precision mechanical stages (Piezo stage, Physik Instruments); experiments were at room conditions. Linearly polarised fs-laser pulses were irradiated onto the surface of the samples using an average laser fluence of $(0.1 - 0.3)$ J/cm^2, which was well below the threshold of glass substrate ablation ∼2 J/cm^2.

After laser exposure, modified ITO on glass substrates were soaked in a 1% vol. HF solution for 5 seconds then rinsed with water to remove the remaining HF solution. Surface morphology was observed by a scanning electron microscope (SEM; JSM-6700F, JEOL) and atomic force microscopy (AFM; Bruker). Energy-dispersive X-ray spectroscopy was carried out using a SEM microscope at 20 kV electron acceleration voltage. Finite Difference Time Domain (FDTD) simulations were carried out using Ansys Lumerical version 2022 R1.

ACKNOWLEDGMENTS

This work was supported by ARC DP190103284, LP190100505 grants, the National Natural Science Foundation of China (NSFC) Grants Nos. 61827826, 62175086, 61960206003, 661805100, and the Interdisciplinary Integration and Innovation Project of JLU (JLUXKJC2021ZZ15). J.H. is grateful for the research stay at Jilin University.

[1]M. Baum, I. Alexeev, M. Latzel, S. H. Christiansen, and M. Schmidt, "Determination of the effective refractive index of nanoparticulate ITO layers," Optics Express **21**, 22754–22761 (2013).
[2]S. Ishibashi, Y. Higuchi, Y. Ota, and K. Nakamura, "Low resistivity indium–tin oxide transparent conductive films. II. Effect of sputtering voltage on electrical property of films," Journal of Vacuum Science & Technology A: Vacuum, Surfaces, and Films **8**, 1403–1406 (1990).
[3]Y.-N. Kim, S.-M. Jeong, M.-S. Jeon, H. Shin, J.-K. Song, and H. Lee, "Reliability assessment of indium tin oxide thin films by accelerated degradation test," J. Electroceramics **17**, 955–958 (2006).
[4]Z. Yu, I. Perera, T. Daeneke, S. Makuta, Y. Tachibana, J. Jasieniak, A. Mishra, P. Bäuerle, L. Spiccia, and U. Bach, "Indium tin oxide as a semiconductor material in efficient p-type dye-sensitized solar cells," NPG Asia Materials **8**, 305 (2016).
[5]S. Xian, L. Nie, J. Qin, T. Kang, C. Li, J. Xie, L. Deng, and L. Bi, "Effect of oxygen stoichiometry on the structure, optical and epsilon-near-zero properties of indium tin oxide films," Optics Express **27**, 28618–28628 (2019).
[6]M. Z. Alam, I. De Leon, and R. W. Boyd, "Large optical nonlinearity of indium tin oxide in its epsilon-near-zero region," J. Electroceramics **352**, 795–797 (2016).
[7]P. Guo, R. D. Schaller, L. E. Ocola, B. T. Diroll, J. B. Ketterson, and R. Chang, "Large optical nonlinearity of ito nanorods for sub-picosecond all-optical modulation of the full-visible spectrum," Nature Communications **7**, 12892 (2016).
[8]S.-N. Ng and S. Juodkazis, "Nanoscale plasmonic printing," Preprints , doi:10.20944/preprints202202.0258.v1 (2022).
[9]S. Lai, Y. Guo, G. Liu, Y. Liu, C. Fu, H. Chang, Y. Wu, and W. Gu, "A High-Performance Ultra-Broadband Transparent Absorber With a Patterned ITO Metasurface," IEEE Photonics Journal **14**, 1–7 (2022).
[10]R. Datta, N. Syed, A. Zavabeti, A. Jannat, M. Mohiuddin, M. Rokunuzzaman, B. Zhang, M. Ataur Rahman, P. Atkin, K. Messalea, M. Ghasemian, E. Gaspera, S. Bhattacharyya, M. Fuhrer, S. Russo, C. McConville, D. Esrafilzadeh, K. Kalantar-Zadeh, and T. Daeneke, "Flexible two-dimensional indium tin oxide fabricated using a liquid metal printing technique," Nature Electronics **3**, 51–58 (2020).
[11]F.-M. Allioux, M. Ghasemian, W. Xie, A. O'Mullane, T. Daeneke, M. Dickey, and K. Kalantar-Zadeh, "Applications of liquid metals in nanotechnology," Nanoscale Horiz. **7**, 141–167 (2022).
[12]H. Morikawa and M. Fujita, "Crystallization and electrical property change on the annealing of amorphous indium-oxide and indium-tin-oxide thin films," Thin Solid Films **359**, 61–67 (2000).
[13]M. Afshar, M. Straub, H. Voellm, D. Feili, K. Koenig, and H. Seidel, "Sub-100 nm structuring of indium-tin-oxide thin films by sub-15 femtosecond pulsed near-infrared laser light," Optics Letters **37**, 563–565 (2012).
[14]C.-W. Cheng and C.-Y. Lin, "High precision patterning of ITO using femtosecond laser annealing process," Applied Surface Science **314**, 215–220 (2014).
[15]C. W. Cheng, C. Y. Lin, W. C. Shen, Y. J. Lee, and J. S. Chen, "Patterning crystalline indium tin oxide by high repetition rate femtosecond laser-induced crystallization," Thin Solid Films **518**, 7138–7142 (2010).
[16]A. Cerkauskaite, R. Drevinskas, A. Solodar, I. Abdulhalim, and P. G. Kazansky, "Form-Birefringence in ITO Thin Films Engineered by Ultrafast Laser Nanostructuring," ACS Photonics **4**, 2944–2951 (2017).
[17]J. Chae, L. Jang, and K. Jain, "High-resolution, resistless patterning of indium-tin-oxide thin films using excimer laser projection annealing process," Materials Letters **64**, 948–950 (2010).
[18]C. J. Lee, H. K. Lin, C. H. Li, L. X. Chen, C. C. Lee, C. W. Wu, and J. C. Huang, "A study on electric properties for pulse laser annealing of ITO film after wet etching," Thin Solid Films **522**, 330–335 (2012).
[19]H. Hosono, M. Kurita, and H. Kawazoe, "Excimer laser crystallization of amorphous indium-tin-oxide and its application to fine patterning," Japanese Journal of Applied Physics, Part 2: Letters **37**, 8–11 (1998).
[20]S. H. Su, H. J. Kong, C. L. Tseng, and G. Y. Chen, "Wet etching mechanism and crystallization of indium-tin oxide layer for application in light-emitting diodes," Japanese Journal of Applied Physics **57**, 1–5 (2018).
[21]S. Wang, Z. Zhou, B. Li, C. Wang, and Q. Liu, "Progresses on new generation laser direct writing technique," Materials Today Nano **16**, 100142 (2021).
[22]Z.-Z. Li, L. Wang, H. Fan, Y.-H. Yu, Q.-D. Chen, S. Juodkazis, and H.-B. Sun, "O-FIB: far-field-induced near-field breakdown for direct nanowriting in an atmospheric environment," Light: Sci. Appl. **9**, 41 (2020).
[23]T. A. F. König, P. A. Ledin, J. Kerszulis, M. A. Mahmoud, M. A. El-Sayed, J. R. Reynolds, and V. V. Tsukruk, "Electrically tunable plasmonic behavior of nanocube-polymer nanomaterials induced by a redox-active electrochromic polymer," ACS Nano **8**, 6182–6192 (2014).
[24]V. Stankevič, G. Račiukaitis, F. Bragheri, X. Wang, E. Gamaly, R. Osellame, and S. Juodkazis, "Laser printed nano-gratings: orientation and period peculiarities," Scientific Reports **7**, 147568 (2017).
[25]S. Rekštytė, T. Jonavicius, D. Gailevičius, M. Malinauskas, V. Mizeikis, E. G. Gamaly, and S. Juodkazis, "Nanoscale precision of 3D polymerisation via polarisation control," Adv. Opt. Mat. **4**, 1209 – 1214 (2016).
[26]L. Grineviciute, S. Ng, M. Han, T. Moein, V. Anand, T. Katkus, M. Ryu, J. Morikawa, M. Tobin, J. Vongsvivut, T. Tolenis, and S. Juodkazis, "Anisotropy of 3D columnar coatings in mid-infrared spectral range," Nanomaterials **11**, 3247 (2021).
[27]E. Gamaly and A. Rode, "Ultrafast re-structuring of the electronic landscape of transparent dielectrics:

new material states (die-met)," Applied Physics A: Materials Science and Processing **124**, 11 (2018).
[28] C. Lopez-Santos, D. Puerto, J. Siegel, M. Macias-Montero, C. Florian, J. Gil-Rostra, V. López-Flores, A. Borras, A. R. González-Elipe, and J. Solis, "Anisotropic Resistivity Surfaces Produced in ITO Films by Laser-Induced Nanoscale Self-organization," Advanced Optical Materials **9** (2021), 10.1002/adom.202001086.
[29] M. M. Islam, K. Ueno, S. Juodkazis, Y. Yokota, and H. Misawa, "Development of interdigitated array electrodes with SERS functionality," Analytical Sciences **26**, 13–18 (2010).
[30] E. Vanagas, I. Kudryashov, D. Tuzhilin, S. Juodkazis, S. Matsuo, and H. Misawa, "Surface nanostructuring of borosilicate glass by femtosecond nJ energy pulses," Appl. Phys. Lett. **82**, 2901–2903 (2003).
[31] A. Žukauskas, M. Malinauskas, A. Kadys, G. Gervinskas, G. Seniutinas, S. Kandasamy, and S. Juodkazis, "Black silicon: substrate for laser 3D micro/nano-polymerization," Optics Express **21**, 6901–6909 (2013).
[32] X.-Q. Liu, L. Yu, Z.-C. Ma, and Q.-D. Chen, "Silicon three-dimensional structures fabricated by femtosecond laser modification with dry etching," Applied Optics **56**, 2157–2161 (2017).
[33] Y. Nishijima, N. To, A. Balcytis, and S. Juodkazis, "Absorption and scattering in perfect thermal radiation absorber-emitter metasurfaces," Optics Express **30**, 4058–4070 (2022).

Appendix A: Additional simulations

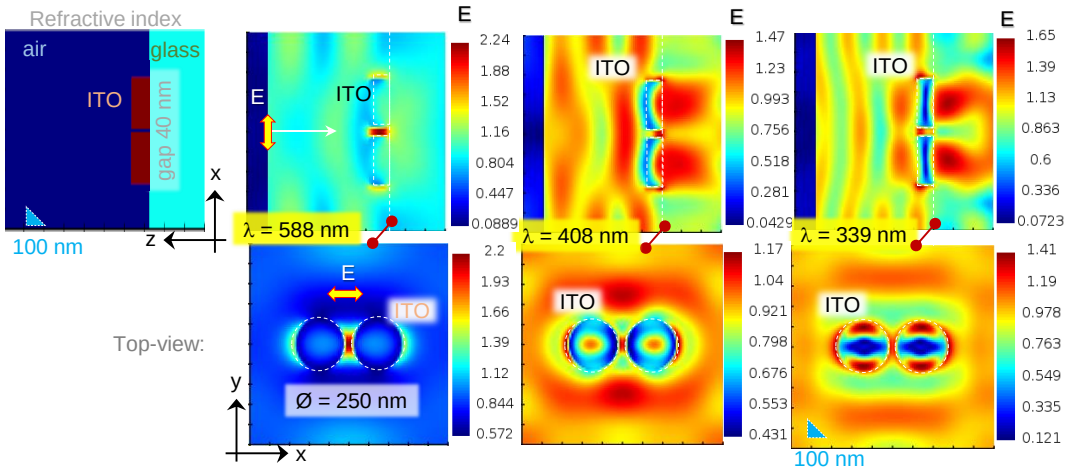

FIG. A1. FDTD calculation of light intensity distribution (within 1 μm^3 volume) for an array of ITO nano-disk pairs; period in xy-plane is $\Lambda_{x,y} = 1$ μm, diameter of ITO disk $2r = 250$ nm, the gap $\Delta x = 40$ nm, height of disk $h = 80$ nm. Light source is a plane wave with a normalised E-field $|E|^2 = 1$. Glass is defined as dielectric with refractive index $n = 1.4$ and the complex refractive index of ITO[23] was added to Lumerical material database as a table. Top-row is the side-view and bottom-row is the top-view E-field enhancement maps.

Light field enhancement for a pair of ITO nano-disks in a periodic pattern (Fig. A1). Examples of selected light field distributions showing the typical nano-gap enhancement mode as well as ones related to the transparency of ITO. Fabry-Pérot and Fano type resonances can be explored with such transparent and electrically conductive ITO metasurfaces, including the design of perfect absorber metasurfaces[33]. The enhancement values are smaller at the UV-visible spectral range (Fig. A1) where extinctions $\sigma_{ab,sc}$ are an order of magnitude smaller compared to the resonance at ~ 850 nm (Fig. 7). The Metal-Insulator-Metal (MIM) surfaces can be made using ITO as metal-base-plate and nano-disk at the top layer with a dielectric of chouce as a I-layer in MIM metasurface.